

Supplementary Information For

**“Large Second Harmonic Generation from Hollow Gold Nanoprisms: Role of Plasmon Hybridization and Structural Effects”**

Bidhan Hazra,<sup>a†</sup> Kamalika Das,<sup>a†</sup> and Manabendra Chandra<sup>a\*</sup>

Department of Chemistry

Indian Institute of Technology, Kanpur, Uttar Pradesh-208016, India

\*Corresponding author, Email: [mchandra@iitk.ac.in](mailto:mchandra@iitk.ac.in)

**Table of Contents**

1. Synthesis of HGNs.....	S2
2. Schematic of the experimental setup for two-photon Rayleigh scattering.....	S3
3. Concentration dependence of two-photon Rayleigh scattering intensities.....	S3
4. Incident power dependence of the second harmonic scattering from HGNs.....	S4
5. Comparison of excitation induced electric-field distribution between HGN I and its solid analogue.....	S4
6. Effect of size and position of the cavity on the excitation induced electric-field distribution and SHG responses of HGN .....	S5
7. Relation between aspect ratio and surface area.....	S6
8. Explanation for the slight discrepancies between the experimental and simulated spectra...S6	
9. Comparison of first hyperpolarizability values ( $\beta'$ ) of HGNs with other nanoparticles .....	S7

## 1. Synthesis of HGNs

All materials were purchased from Sigma-Aldrich. Milli-Q (18 M $\Omega$ -cm at 25C) water was the solvent for all experiments.

Hollow gold nanoprisms (HGN) were prepared following a method already reported in literature.<sup>S1, S2</sup> The HGNS are synthesized in two steps. In the first step, small silver nano-seeds (4-5 nm) are synthesized. The second step involves the preparation of HGN *via* sacrificial galvanic replacement method. A short description of the stepwise synthesis is presented below.

Step I : Synthesis of Ag nanoseed. 20 mL water was taken in a conical flask and placed on a magnetic stirrer. A magnetic bead was placed in the conical flask and stirred slowly. 500  $\mu$ L of  $10^{-2}$  M AgNO<sub>3</sub> was added drop by drop, with continuous stirring. After proper mixing for 30 sec, 200  $\mu$ L of  $2.5 \times 10^{-2}$  M trisodium citrate was added drop wise. This was followed by addition of 60  $\mu$ L of  $10^{-1}$  M freshly prepared ice cold NaBH<sub>4</sub> drop by drop and stirring was stopped within 10 sec. The color of the solution gradually became transparent-yellow. The solution was kept undisturbed in dark for 4 hours before using it for seed mediated growth process of HGNS.

Step II: Growth of HGNS. We prepared four different HGNS by sacrificial galvanic replacement of silver seed. 490 mg CTAB was taken in a conical flask and then 45 mL water was added to it. The solution was sonicated and slightly warmed to dissolve CTAB. When the CTAB was totally dissolved, the conical flask was kept on a magnetic stirrer under constant slow stirring. 2 mL of  $10^{-2}$  M AgNO<sub>3</sub> was slowly added into this CTAB solution. After proper mixing, 300  $\mu$ L of  $10^{-2}$  M HAuCl<sub>4</sub> was added (drop by drop) and the color of the solution changes from colorless to yellow-brown. 320  $\mu$ L of  $10^{-1}$ M of Ascorbic acid was added drop by drop. The solution turns colorless. We added another 300  $\mu$ L of  $10^{-2}$  M HAuCl<sub>4</sub> and 320 $\mu$ L of  $10^{-1}$  M of ascorbic acid (AA) into this colorless solution successively and rapidly. Immediately after the second addition of AA, different amount of silver seed was added at a time. Volume of seed solution added for synthesizing four different HGNS were 2.5mL (HGN-I), 2mL (HGN-II), 1.5 mL (HGN-III), and 1 mL (HGN-IV).

## 2. Schematic of the experimental setup for two-photon Rayleigh scattering measurement.

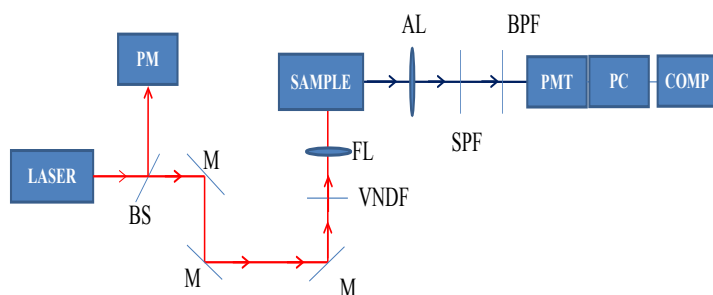
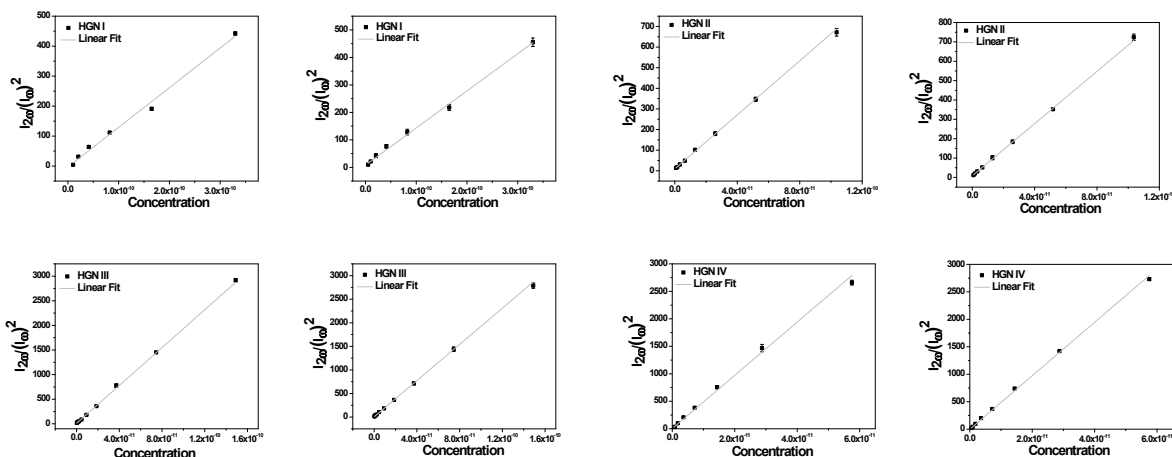


**Figure S1.** Schematic of the TPRS experimental setup is shown. AL: aspherical lens; BPF: band pass filter; BS: beam splitter; COMP : computer; FL: focusing lens ; LASER: mode-locked solid-state Ti: sapphire laser with 80 MHz repetition rate and  $\sim 100$  fs pulse width; M:mirror ; PC : photon counter; PM: power meter ; PMT: photomultiplier tube; SPF: short pass filter; VNDf: variable neutral density filter.

## 3. Concentration dependence of two-photon Rayleigh scattering intensities

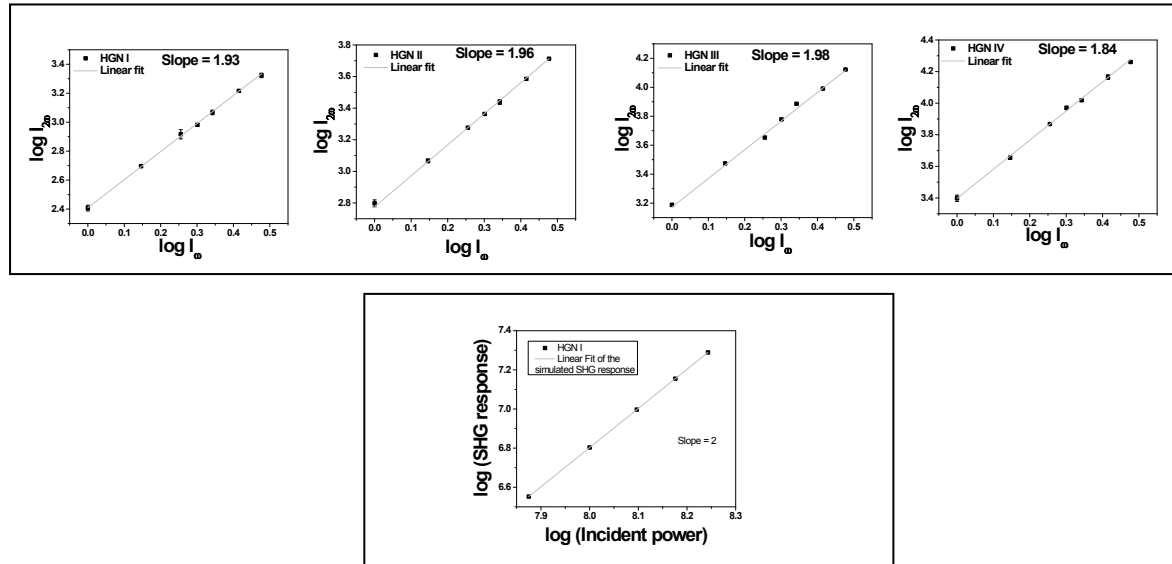
The second harmonic photon counts were recorded as a function of particle concentration. The two-photon signal intensity normalized to the square of the fundamental intensity is increase linearly with concentration. This linearity is a signature of an incoherent SHG process.



**FigureS2.** Concentration dependencies of two-photon Rayleigh scattering from four different HGNs are shown. Two different measured data sets are shown for each HGNs.

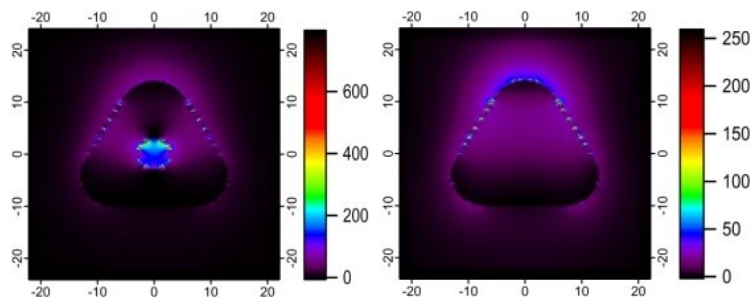
#### 4. Incident power dependence of the second harmonic scattering from HGNs

Incident power dependence of the experimentally detected (or numerically simulated) scattered photons at the second harmonic frequency was investigated. The order of the nonlinear process was confirmed from the slope of the  $\log(I_{2\omega})$  vs  $\log(I_{\omega})$  plot.



**FigureS3.** (Top) Experimental power dependence plots obtained for the HGNs. A slope of  $\sim 2$  confirms a two photon process in each case. (Bottom) Power dependence plots obtained for the FDTD simulated SHG response from HGN I. A quadratic power dependence confirms SHG process.

#### 5. Comparison of excitation induced electric-field distribution between HGN I and its solid analogue



**FigureS4.** Electric field distributions at corresponding absorption maxima of HGN I and its solid analogue are shown. It can be seen from the scale bars that the maximum field enhancement ( $|E|^2/|E_0|^2$ ) is much higher for HGNs. Also, it is clear from the plot that the cavity enhances the field significantly

## 6. Effect of size and position of the cavity on the excitation induced electric-field distribution and SHG responses of HGN

We have numerically studied the effect of increasing cavity diameter on the local electric field enhancement ( $|E|^2/|E_0|^2$ ) and SHG in HGNs. We took HGN IV as a case study. We increased the diameter of HGN IV from  $\sim 5$  nm to 15 nm keeping everything else the same (also the center of the cavity remained at the center of mass of the prism). We see  $\sim 50\%$  increase in the  $|E|^2/|E_0|^2$  value. In the next step we shifted this 15 nm cavity toward the tip by 10 nm and we see another  $\sim 50\%$  increase in the  $|E|^2/|E_0|^2$  value. These increments are due to stronger coupling among plasmon modes supported by the cavity and the other outer surfaces. When we simulated the SHG responses from the above mentioned three structures, we found the same trend as we saw for the E-field. Thus, it is quite evident that a careful optimization of the HGN structure can indeed lead to unprecedented large optical nonlinearity.

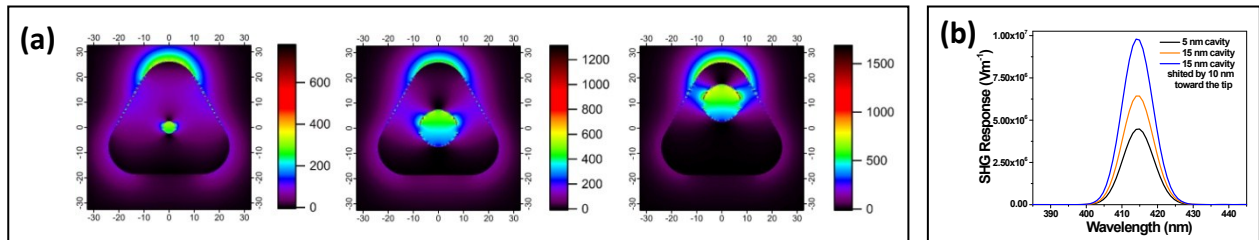
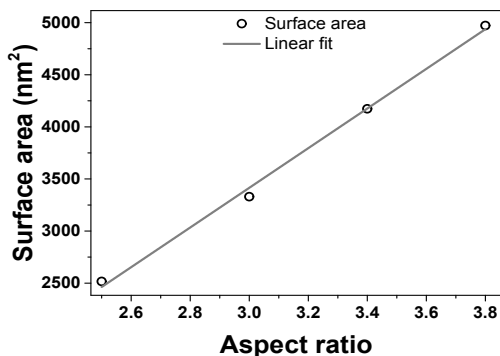


**Figure S5.** (a) Electric field distribution of HGN IV and two other HGNs, one with higher cavity diameter (15 nm) and other with higher cavity diameter (15 nm) shifted cavity position (10 nm toward the tip). The increase in the  $|E|^2/|E_0|^2$  value upon increasing the cavity diameter or decreasing tip to cavity distance is obvious. (b) Calculated SHG spectra of the HGNs depicted in (a) are shown. Concomitant increase in the SHG response with the electric field enhancement is apparent.

## 7. Relation between aspect ratio and surface area of HGNs



**FigureS6.** Plot of surface area as a function of aspect ratio is depicted. Linearity of the variation is very clearly visible.

## 8. Explanation for the slight discrepancies between the experimental and simulated spectra

The simulated absorption spectra of all of the HGNs are a little red-shifted as compared to their experimental counterparts. This small difference in the LSPR maxima of the experimental and the theoretical spectra is most likely due to a difference in the actual dielectric constants of the solvent medium in the actual sample and that used in the FDTD simulation. Also, a finer (<1 nm) mesh size would probably result in better match between the theoretical and experimental spectra. However, the computational cost goes up significantly when the mesh size is reduced.

We also note that the simulated spectral line-widths are systematically lower than the experimental line widths. This is quite understandable. In the simulations, only one isolated HGN is used and the dimension that is used to simulate the LSPR spectra of HGNs are just the average dimension obtained from the TEM analyses. However, the actual colloidal dispersion has finite size distribution that leads to inhomogeneous broadening of the spectra. Also, the synthesized HGNs contain various degrees of defects, which too contribute to the overall broadening of the spectral line widths in the experiment than in the simulations.

## 9. Comparison of first hyperpolarizability values ( $\beta'$ ) of HGNs with other nanoparticles

Comparison of SHG enhancements in case of nanoparticles is not very straightforward as, unlike molecular chromophores, nanoparticles suffer from various defects and heterogeneities. However, a moderate platform for comparing SHG enhancements from nanoparticles can be obtained by normalizing the first hyperpolarizability values with respect to the number of

atoms (i.e.,  $\beta' = (\beta^2/\text{atom})^{1/2}$ ). In the present paper, we have described the first hyperpolarizability values of the HGNs both as  $\beta/\text{particle}$  and  $\beta'$ . Some previous reports too, have provided the first hyperpolarizability values of different nanostructures in terms of  $\beta'$ . We have now compared our measured  $\beta'$  values with those reported ones (also, in some cases we have determined  $\beta'$  values from the reported  $\beta$  values and the nanoparticles' dimensions). The comparison is presented in the table below.

Table S1. Comparison of first hyperpolarizability values ( $\beta$ ) of HGNs with other nanoparticles

Sample	Aspect Ratio	$\beta' = (\beta^2/\text{atom})^{1/2}$
	[AR]	( $\times 10^{-30}\text{esu}/\text{atom}^{1/2}$ )
HGN I	$2.5 \pm 0.1$	$1461.15 \pm 107.04^{(a)}$
HGN II	$3.0 \pm 0.2$	$3780.66 \pm 37.94^{(a)}$
HGN III	$3.4 \pm 0.1$	$5433.25 \pm 3.91^{(a)}$
HGN IV	$3.8 \pm 0.3$	$7549.25 \pm 12.14^{(a)}$
NR1	1.7	$50^{(S3)}$
NR2	1.9	$68^{(S3)}$
NR3	2.5	$77^{(S3)}$
NR4	2.7	$90^{(S3)}$
NR5	3.8	$103^{(S3)}$
SGN	NA	$492^{(S3)}$
Hollow Gold Nanosphere-I	3.56	$619^{(S4)}$
Hollow Gold Nanosphere -II	6.88	$2060^{(S4)}$
Gold Nanoparticle	NA	$2800 \pm 500^{(S5)}$

(a) The present study.

## References

- S1. D. Senapati, T. Senapati, P. S. Wate, R. Kanchanapally, Z. Fan, A. K. Singh and P. C. Ray, *Chem. Commun.*, 2012, **48**, 6034-6036.
- S2. B. Hazra, K. Das, S. Das Chakraborty, M. S. Verma, M. M. Devi, N. K. Katiyar, K. Biswas, D. Senapati and M. Chandra, *J. Phys. Chem. C*, 2016, **120**, 25548-25556.
- S3. A. Singh, A. Lehoux, H. Remita, J. Zyss and I. Ledoux-Rak, *J. Phys. Chem. Lett.* 2013, **4**, 3958–3961.
- S4. M. Chandra, A. M. Dowgiallo and K. L. Knappenberger Jr., *J. Phys. Chem. C*, 2010, **114**, 19971– 19978.
- S5. F. W. Vance, B. I. Lemon and J. T. Hupp, *J. Phys. Chem. B*, 1998, **102**, 10091–10093.